Stable lotus leaf-inspired hierarchical, fluorinated polypropylene surfaces for reduced bacterial adhesion

Md Imrul Kayes[a,1], Anthony J. Galante[a,1], Nicholas A. Stella[b], Sajad Haghanifar[a], Robert M.Q. Shanks[b], Paul W. Leu[a,c,d,*]

[a] Department of Industrial Engineering, University of Pittsburgh, 3700 O'Hara, Benedum Hall of Engineering, Pittsburgh, PA, 15261, United States
[b] Department of Ophthalmology, Charles T. Campbell Laboratory for Ophthalmic Microbiology, University of Pittsburgh School of Medicine, 203 Lothrop Street, Pittsburgh, PA 15213, United States
[c] Department of Mechanical Engineering, University of Pittsburgh, 3700 O'Hara, Benedum Hall of Engineering, Pittsburgh, PA 15261, United States
[d] Department of Chemical Engineering, University of Pittsburgh, 3700 O'Hara, Benedum Hall of Engineering, Pittsburgh, PA 15261, United States

A R T I C L E I N F O

A B S T R A C T

Polypropylene (PP) is used in a wide variety of medical components, but is susceptible to bacteria surface colonization and biofilm formation, which lead to infections and inflammations. In this study, we report on the micro-/nanostructuring and surface functionalization of PP substrates through various oxygen and fluorine reactive ion etching (RIE) treatments and their effects on wettability and bacteria adhesion. We found that oxygen treatment creates a hydrophilic surface that reduces bacteria adhesion by 68.7% compared to the control, but additional nanostructuring reduces the surface's anti-biofouling properties due to increased microscale roughness and air pockets that reduce the effectiveness of the liquid barrier. We demonstrate that a fluorine etch chemistry may be utilized to create lotus leaf-inspired, low surface energy, hierarchical microstructure/nanofibrils in PP. Due to the low surface energy and hierarchical morphology, the surface exhibits lotus-leaf wetting (high contact angle ~155° and low contact angle hysteresis < 10°) where water droplets easily roll off the surface in contrast to other PP samples. The lotus leaf-inspired hierarchical, fluorinated surfaces exhibit a 99.6% reduction of *E. coli* cell adhesion compared to untreated PP. These surfaces demonstrate water contact angle stability over a week in contrast to hydrophilic samples, where the contact angle degrades after just a few days. These new surfaces may help reduce the spread of infections from various plastic medical components without the need for the loading of antibacterial agents that eventually deplete from the surface.

1. Introduction

Plastics are used in a wide range of medical components such as prosthetics, implants, catheters, and syringes, due to their chemical resistance, versatility in manufacturing, high specific strengths, and low cost [1]. However, contaminating bacteria can attach to plastic surfaces and grow and form biofilms that lead to healthcare associated infections [2]. The consequences on patients and their families are serious, as infections can extend hospital stays, create long-term disability, increase healthcare costs, and even result in unnecessary deaths [3,4]. In the United States alone, there are 90,000 deaths associated with healthcare-associated infections every year [5]. These issues are even worse in developing countries where resources and accountability are poor [6].

Bacteria cause infections by attaching to a surface and forming organized and multicellular biofilms. Two strategies for creating antibacterial surfaces are (1) bactericidal surfaces that kill bacteria cells that come in proximity of or contact the surface and (2) anti-biofouling surfaces that make the bacterial attachment process difficult. In this study, we focus on modifying polypropylene (PP), which is a thermoplastic suitable for use in clinical environments due to its unique rigidity, chemical solvent resistance, and ability to withstand high temperatures compared to other polymers [7]. PP is commonly used for injectors, syringes, medical packaging and cases for contact lenses [8–12] and is expected to be the fastest growing plastic for medical packaging [13]. Many bactericidal PP surfaces have been studied by

---

* Corresponding author at: Department of Mechanical Engineering, University of Pittsburgh, 3700 O'Hara, Benedum Hall of Engineering, Pittsburgh, PA 15261, United States.
E-mail address: pleu@pitt.edu (P.W. Leu).
[1] Md Imrul Kayes and Anthony Galante contributed equally to this work.

incorporating silver nanoparticles-zeolite plastics [14], copper nanoparticles [15,16], and silver nanoparticles [17,18]. However, nanoparticles are easily removed by abrasion [19,20] and the metal ions eventually leach out of the surface completely, rendering the surface sterile against bacteria. Metal ions may also be toxic to aquatic organisms and the environment [21,22]. Furthermore, bactericide agents must be used in high concentration because many bacteria can sustain growth in low concentrations [23]. Anti-biofouling PP surface modifications have been investigated to combat these issues. PP membranes have been fabricated by the UV-induced grafting of zwitterionic antifouling polymers and demonstrated a 77% reduction in *Escherichia coli* (*E.Coli*) adhesion [24]. Anti-biofouling PP surfaces have also been prepared by thermal annealing to create microscale patterns of rice that reduce the adhesion of *E. coli* by 53% compared to controls [25].

In this study, we examined how different reactive ion etching (RIE) processes affect the anti-biofouling properties of PP samples. Our reactive ion etching method provides a single step approach without the need for patterning or the incorporation of additional materials. We studied how different oxygen and fluorine reactive ion etching (RIE) treatments affect the surface chemistry, morphology, wettability, and bacteria adhesion of PP. We found that a light power oxygen etching treatment creates a hydrophilic surface that reduces bacteria adhesion of *Escherichia coli* (*E. coli*) by 68.7% compared to untreated PP. Etching a PP surface with high power oxygen creates a surface with about the same surface energy, but nanofibril structures with microscale roughness. These structures exhibit increased bacteria adhesion due to a combination of greater microscale roughness and air pockets that reduce the effectiveness of the liquid barrier. In contrast, we demonstrate substantially reduced bacteria adhesion through lotus-leaf-inspired low surface energy, hierarchical microstructure/nanofibrils in PP. These surfaces exhibit lotus-leaf-like wetting with high static water contact angle (~155°) and low hysteresis (< 10°). Water droplets easily roll off these surfaces as opposed to the other PP samples. Furthermore, these lotus-leaf-like surfaces reduce *E. coli* by 99.6% compared to untreated control samples. These surfaces demonstrate water contact angle stability over a week in contrast to hydrophilic samples, where the contact angle degrades after just a few days.

2. Experimental section

2.1. Materials

PP sheets were purchased from an online vendor (Small Parts), which have a standard tolerance and meet ASTM D4101-PP0112 specifications [26]. The thickness of the PP sheet was 1.57 mm. Electronic grade acetone (99.5%), methanol (99.9%) and isopropyl alcohol (99.5%) were bought from VWR. Diiodomethane (99%) was bought from Sigma-Aldrich. Deionized water was obtained from a Millipore Academic A10 system with total organic carbon below 40 ppb.

2.2. Sample preparation

Circular coupons of 12.7 mm diameter were made from a PP sheet using a custom-made hole punch. Afterwards, the samples were cleaned with acetone, methanol, and isopropyl alcohol and dried with nitrogen gas. All samples, including the control, were cleaned with a low power argon plasma (Diener Electronic GmbH) using diffusion process plasma cleaning. The plasma clean parameters for all samples were set to power = 20 W, pressure = 100 mTorr, flow rate = 30 sccm and duration = 70 s. Then, experimental samples were treated by RIE (Trion III). Two types of samples were prepared by oxygen treatment. Both oxygen treatments were performed under pressure = 100 mTorr, O_2 flow rate = 98 sccm, and duration = 120 s. However, one treatment had high power (HP) of 200 W and the other had a low power (LP) of 25 W. The fluorinated samples were initially treated with oxygen for 70 s and then treated with CF_4 and SF_6 gasses in order to maximize fluorination

at power = 200 W, pressure = 250 mTorr, CF_4 flow rate = 86 sccm, SF_6 flow rate = 52 sccm, and duration = 1800 s (or 30 min).

2.3. Surface characterization

2.3.1. Morphology characterization

The physical morphology of PP surfaces was characterized by scanning electron microscopy (SEM, Zeiss Sigma 500 VP) and atomic force microscopy (AFM, Multimode SPM with a Digital Instruments Nanoscope III controller). For SEM imaging, the samples were sputter coated with 7 nm gold/palladium (80:20) using a sputter coater (Hummer), as the polymer samples were non-conductive. For AFM, the PP surfaces were imaged in tapping mode, using silicon nitride tips to assess surface topography and roughness in 20 μm by 20 μm areas. The AFM tip had a radius of 8 nm, and the total tip height was 12–18 μm. Data analysis was performed with Digital Instruments version v720 and Gwyddion software. Additionally, dimensional stability was tested with the ASTM D1204 standard (except with 3 in. by 3 in. samples) by comparing the dimensions of samples before and after RIE treatment [27]. Measurements of the sample width and length before and after plasma treatments were conducted using a digital vernier scale caliper.

2.3.2. Contact angle measurements and surface energy calculation

Static water contact angles (WCA) for all the surfaces were measured using a video contact angle goniometer (VCA 2000 Optima XE). This goniometer utilizes a precision camera and advanced PC technology to capture static or dynamic images of the droplet and determine tangent lines for the basis of contact angle measurement. Contact angle measurements were taken in ambient air at 22–25 °C and 20–30% relative humidity. Contact angle measurements were taken from 5 μl droplets of deionized water. Similarly, the hysteresis was tabulated for each treatment by measuring the advancing and receding contact angles during syringe controlled water dispersion and withdrawal, respectively. Hysteresis is defined as the difference between the advancing and receding contact angle. The fractional surface areas in analyzing different wetting states were calculated using MATLAB Image Processing Toolbox.

2.3.3. X-ray photoelectron spectroscopy

All samples were analyzed by X-ray photoelectron spectroscopy (XPS, Thermo Fisher ESCALAB 250 Xi multichannel) with monochromatic Al K radiation. XPS was performed at an acceleration voltage of 15 kV with an emission current of 15 mA, in a residual vacuum of approximately 1×10^{-9} Torr. The analyzer was used in fixed analyzer transmission (FAT) mode. The spectra were taken from two areas on each sample, and a minimum of two replicate samples were analyzed for each recipe. Sample surface compositions were determined from the average of these measurements.

2.4. Bacterial adhesion experiments

Adhesion to surfaces was tested using a fluorescent bacterial strain. To generate fluorescent bacteria, *E. coli* K-12 strain W3110 was transformed by electroporation with GFP expressing plasmid pGFPmut2 [28,29]. Cultures of the fluorescent *E. coli* were grown in 5 ml of LB broth at 30 °C for 18–20 h with aeration and normalized to $OD_{600} = 0.1$ using saline (NaCl 0.9%) in a spectrophotometer (SpectraMax M3) [30]. Coupons were glued to the bottoms of the wells of 12 wells plates as previously described and the silicon sealant was allowed to dry for 30 min [31]. The wells were then filled with 2.5 ml of the fluorescent bacteria in saline. After 30 min at 37 °C, the saline was removed, and the coupons were rinsed three times with 2.5 ml of saline to remove non-adhered bacteria. The exposed coupon surface was then placed under a coverslip and observed by fluorescent microscopy (Nikon TE2000-E microscope with a Photometrics CoolSNAP HQ-camera and a 20× objective). NIS-Elements 3.2 software was used to obtain digital

images that were then analyzed for the number of attached bacteria using ImageJ software (NIH). In some cases, a few loosely attached bacteria cells were observed, which were moving on the surface. These bacteria were manually calculated and subtracted from the counts obtained from ImageJ counts and represented < 10% of the total bacteria in all cases. The field of view for each picture was 350 μm by 265 μm. Approximately 10 images were taken across the mid-point of each coupon from side to side to gain representative data and eight separate coupons of each type were read for each experiment.

3. Results and discussion

3.1. Fabrication

In this study, both oxygen plasma treated hydrophilic and fluorine treated hydrophobic PP samples were investigated. Oxygen plasma tends to render the surfaces hydrophilic, while fluorine tends to make the surface hydrophobic. Both types of RIE treatments were studied as surface wetting properties have been observed to have a significant impact on bacterial adhesion [32] and both hydrophilic [33] and hydrophobic [34] surface functionalization have been utilized previously to reduce bacterial adhesion. RIE recipes of different samples were tuned for a range of observable wetting results from plasma modified PP. The RIE process modifies the surface morphology from a combination of physical and chemical reactions with the substrate due to the prolonged surface bombardment of activated ions in a controlled environment.

We varied the power to prepare two types of oxygen treated samples having similar hydrophilicity, but different surface morphology. Initially, three types of fluorination recipes were evaluated, using only CF_4, only SF_6, and a combination of both gasses, to prepare the hydrophobic samples. Different durations of 10, 30, and 60 min were also tested. An optimized recipe for realizing maximum superhydrophobicity (in terms of highest contact angle) was obtained when CF_4 and SF_6 were set at 86 and 52 sccm, respectively, for a 30 min duration.

3.2. Surface characterization

The surface topography and surface chemistry was altered by plasma ion bombardment during the RIE process. SEM images of the PP samples are shown in Fig. 1, which demonstrate the difference in surface morphology of the control (Fig. 1a), LP oxygen sample (Fig. 1b), HP oxygen sample (Fig. 1c), and fluorinated sample (Fig. 1d). Both the (i) top view and (ii) 75° tilted view of each sample are shown. The surface of the untreated control samples and the LP oxygen treated samples look similar and are both relatively smooth. On the other hand, the surface of HP oxygen treated samples show nanofibril structures. The HP oxygen PP surface morphology consists of dense forests of nanofibrils about 40 nm diameter and 1 μm height. The fluorinated samples have hierarchical features, with microstructures of about 1 μm in height and nanofibrils of about 30 nm diameter of about 0.5 μm height. These nanofibrils are not as dense as the HP oxygen treated samples.

The surface morphologies of the four types of samples were further characterized by AFM (Fig. 2a). The surface morphology was characterized by the root mean square (RMS) roughness and the power spectral density function. The RMS value of the surface roughness of the control, LP oxygen treated, HP oxygen treated, and fluorinated samples were 20, 37, 230, and 154 nm respectively. While the untreated and LP oxygen treated samples are relatively flat, the HP oxygen treated samples and the fluorinated samples have much more roughness. Fig. 2b plots the roughness power spectral density as a function of the roughness wavelength. The HP oxygen sample has more roughness across all length scales compared to the LP oxygen sample. For length scales below 1 μm, the surface is self-affine or fractal [35] as the power spectral density has a power-law dependence on the spatial frequency
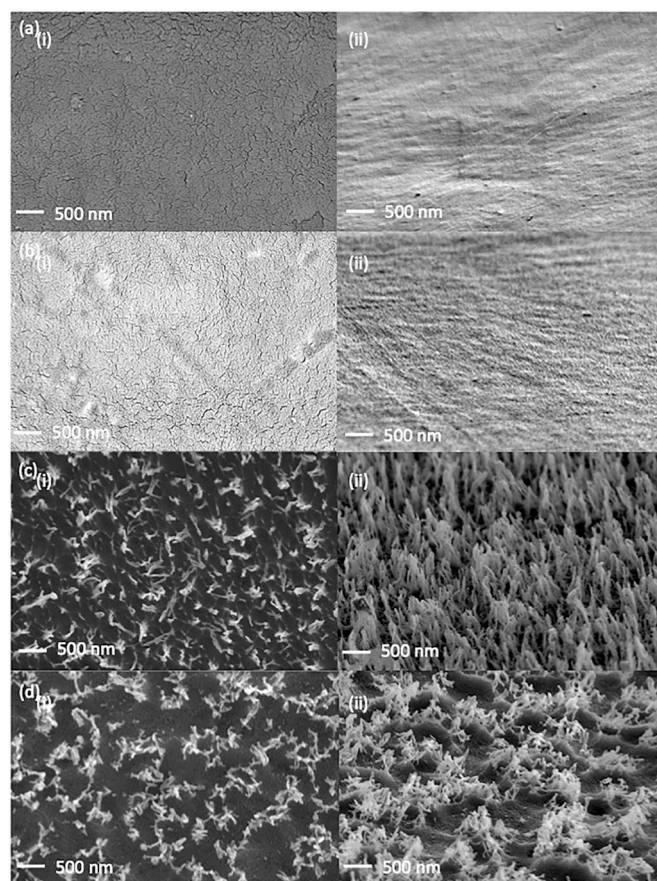
Fig. 1. SEM images of different samples: (a) Control, (b) LP oxygen, (c) HP oxygen, and (d) fluorinated samples. (i): Top view and (ii): 75° tilted. All images were taken at same magnification level.

of roughness. For roughness wavelengths above 1 μm, the power spectral density is fairly flat. In contrast, the fluorinated PP samples are self-affine across almost the entire roughness wavelengths shown, ranging from 20 μm down to 100 nm. This self-affinity across multiple length scales is also present in lotus leaves [36] and why we describe these surfaces as hierarchical.

The dimensional stability of the PP was also evaluated after RIE. Morphological changes may occur in thermoplastics from high temperature treatments due to the mismatch between the thermo-elastic properties of the polymer matrix and fibril structures [37]. The mean dimensional changes of LP oxygen treated, HP oxygen treated, and fluorinated samples were 0.03% ± 0.05%, −0.42% ± 0.23%, and 0.13% ± 0.10%, respectively. All types of samples were dimensionally stable with negligible changes in length and width after the corresponding reactive ion etching treatments.

Fig. 3 shows static water contact angle (WCA) results on the four different types of samples during WCA. The static WCA was measured for 3 samples of each type at 3 random spots per sample. The numbers in the figure denote the mean and standard error among treatments. The WCA was 98 ± 0.9° for the control samples where the ± 0.9° refers to the standard error of the 9 measurements. Both types of samples prepared by oxygen treatment were hydrophilic. The LP oxygen treated samples had WCA of 51 ± 1.3° and HP oxygen treated samples had WCA of 72 ± 1.5°. On the other hand, the fluorinated samples are superhydrophobic with a WCA of 156 ± 0.6°.

The advancing and receding contact angle of the four samples were further characterized. Fig. 4 shows the results of this characterization where 3 samples were again measured 3 times each. The hysteresis is the difference between the advancing and receding contact angles. The
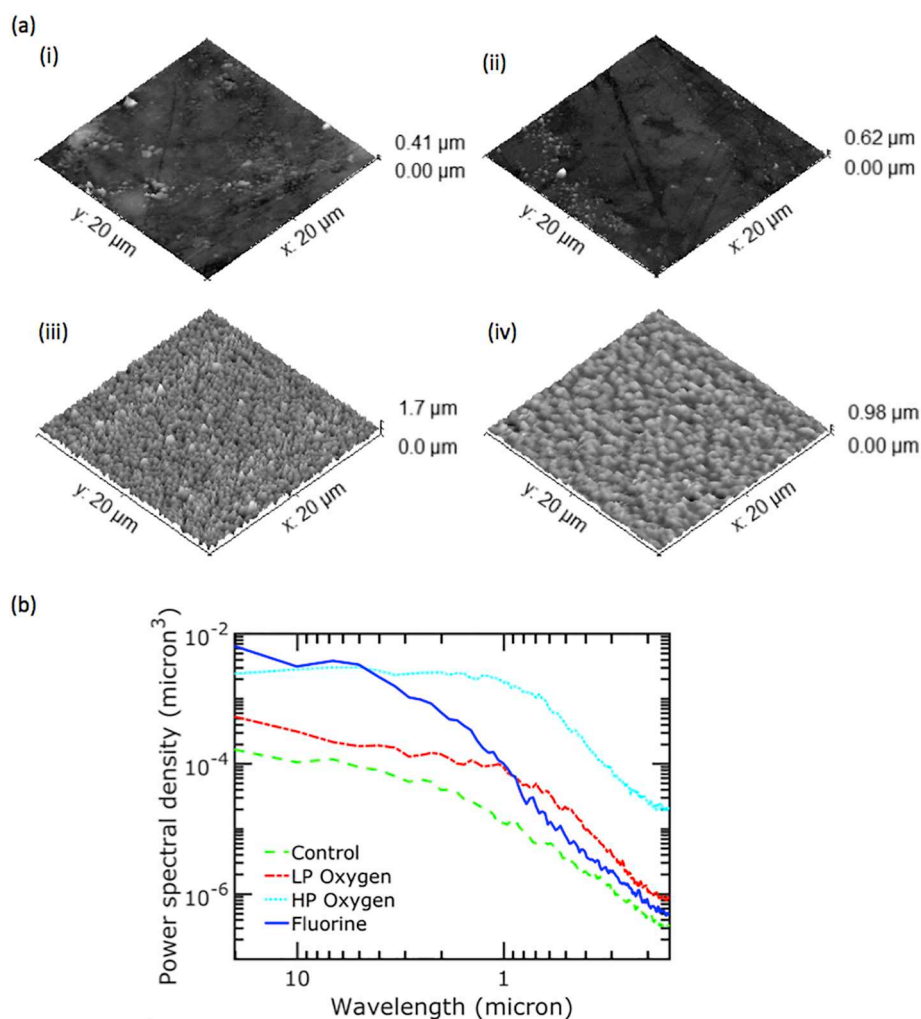
Fig. 2. (a) 3-D plots by AFM show physical surface at microscale of different samples. (i) Control, (ii) LP oxygen, (iii) HP oxygen, and (iv) fluorinated, (b) Power spectral density of four samples as a function of roughness wavelength.

hysteresis was fairly high for the control sample and the oxygen treated samples, which are indicative of strong adhesion between the water and PP. These three samples may all be turned upside down with the water droplet still adhering to the substrate (Fig. 4 images). On the other hand, the contact angle hysteresis for the superhydrophobic samples was approximately < 10°, suggesting that the adhesion force between the liquid and surface is weak [38]. The water droplets easily roll off these surfaces with the slightest tilt. This combination of high WCA and low hysteresis is referred to as the lotus leaf wetting state and an indicator of self-cleaning ability [38].

The total surface energy of different samples was calculated from Fowkes method experiments, where the contact angle of diiodomethane Θ_{DIM} and water Θ_{H20} were used to calculate the total surface energy values (Table 1). Static contact angles of diiodomethane (DIM), a purely dispersive liquid, were measured together with those of water, a highly polar liquid [39]. The independent dispersion and polar surface energy components for each sample type are calculated using Young's and Dupre's definition of adhesion equations. These quantities are summed for the overall surface free energy [40,41].

Young's contact angles were obtained from the observed contact angle values and corresponding wetting state equations. For the Wenzel wetting state,

RIE Recipe	Control	Low Power Oxygen	High Power Oxygen	Fluorinated
Contact Angle	98° ± 0.9°	51° ± 1.3°	72° ± 1.5°	156° ± 0.6°
Images				

Fig. 3. Contact angle of different samples and representative images of the water.
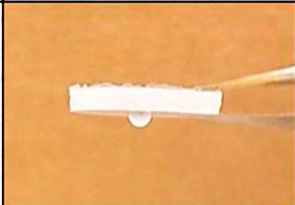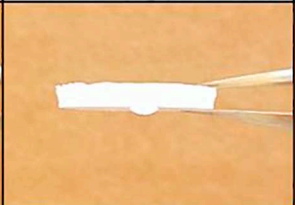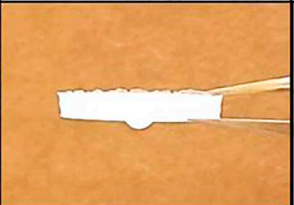
RIE Recipe	Control	Low Power Oxygen	High Power Oxygen	Fluorinated
Advancing CA	106.0° ± 1.2°	78.4° ± 3°	90.5° ± 3.1°	156.5° ± 1.1°
Receding CA	62.8° ± 3.2°	18.2° ± 2.9°	20° ± 1.4°	147.5° ± 1.2°
Hysteresis	43.1° ± 3.2°	60° ± 3.7°	70.5° ± 3.4°	8.9° ± 1.1°
Images				

Fig. 4. Contact angle hysteresis of different samples and images of 180° tilted sample.

Table 1
Diiodomethane (DIM) contact angle, water contact angle, surface energy of different samples, roughness ratio factor, solid-liquid fractional surface area, and Young's contact angle.

	r	f	Θ_Y (degrees)	Θ_{DIM} (degrees)	Θ_{H20} (degrees)	Ω_S (mN m^{-1})
Control	1.03	1	98.2	60 ± 2.2	98 ± 0.9	28.4 ± 2
LP oxygen	1.11	1	55.3	62 ± 2.0	51 ± 1.3	46.7 ± 2.3
HP oxygen	3.02	0.38	36	13.5 ± 3.0	72 ± 1.5	59.6 ± 2.2
Fluorinated	2.63	0.21	103.2	110 ± 4.4	156 ± 0.6	12.9 ± 2.2

$$\cos(\theta_W) = r \cos(\theta_Y)$$

where θ_W is the observed contact angle in the Wenzel wetting state and θ_Y is the Young's contact angle. In the Cassie Baxter wetting state,

$$\cos(\theta_{CB}) = r * f * \cos(\theta_Y) - (1 - f)$$

where θ_{CB} is the observed contact angle in the Cassie Baxter wetting state. r is the roughness ratio factor and f is the solid-liquid fractional surface area where 1- f is the solid-air fractional surface area.

The flat control and LP oxygen samples are in the Wenzel wetting state due to the relatively flat surfaces. In the Wenzel wetting state, the roughness parameter enhances the intrinsic wetting property of a surface, while in the Cassie-Baxter wetting state the roughness always make the surface more hydrophobic. The observed wetting behavior of the HP oxygen samples suggests that they are in the Cassie-Baxter wetting state. In addition, the superhydrophobic behavior of the fluorinated samples indicate the surface must be in the Cassie-Baxter wetting state. The mean and standard error of these values are shown in the table. The surface energy, Ω_S is the sum of the dispersive and polar component of surface energy. The fluorinated samples are superhydrophobic due to a combination of low surface energy and hierarchical surface structures. In contrast, the oxygen treated samples have high surface energy, explaining the lower static contact angles and higher hysteresis.

Table 2 summarizes our XPS results (Supplemental Figs. 1–4). It was observed the fluorinated samples had 55% fluorine on the surface. The untreated samples did not have any fluorine, while the LP oxygen

treated samples had a very small amount (0.85%). However, the HP oxygen treated samples had higher amount of fluorine (5%) compared to the control and LP oxygen treated samples. The presence of fluorine in our HP and LP oxygenated samples are possibly due to the presence of fluorine in the chuck and backstreaming of oil during the RIE process.

Contact angles were measured over a week of time for all samples to check their stability. The mean contact angles at different time points are shown in Fig. 5. The standard error was always within 2° for control, LP oxygen treated and fluorinated samples, while it was a little higher (4°) for HP oxygen treated samples. The LP and HP oxygen treated samples were observed to have decreasing hydrophilicity in ambient conditions after just a few days. This is likely due to particulates landing on the high energy surface. However, the fluorinated samples demonstrated stable superhydrophobicity over a week as the mean contact angle was always higher than 146°. The fluorinated

Table 2
XPS surface chemical analysis of the various surfaces.

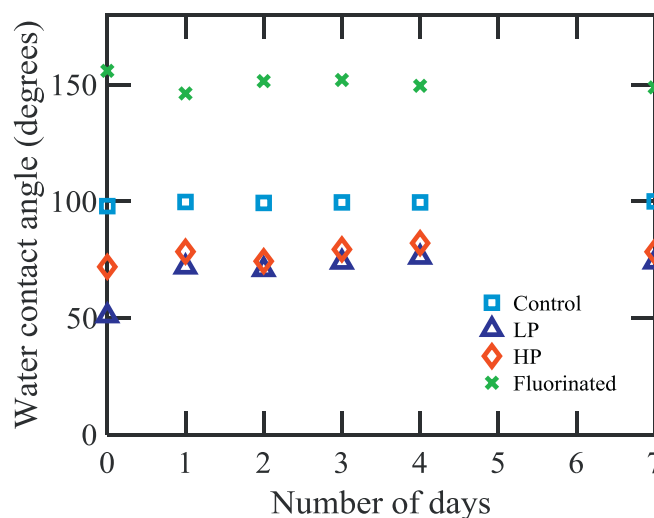| Atomic %						
Name	C 1s	O 1s	N 1s	F 1s	Si 2s	Al 2p
Control	88.35	9.55	0.73	0	1.37	0
LP oxygen	82.16	13.89	0.75	0.85	0.97	1.38
HP oxygen	66.39	21.09	1.38	5.51	1	4.63
Fluorinated	43.19	0.86	0.68	55.27	0	0

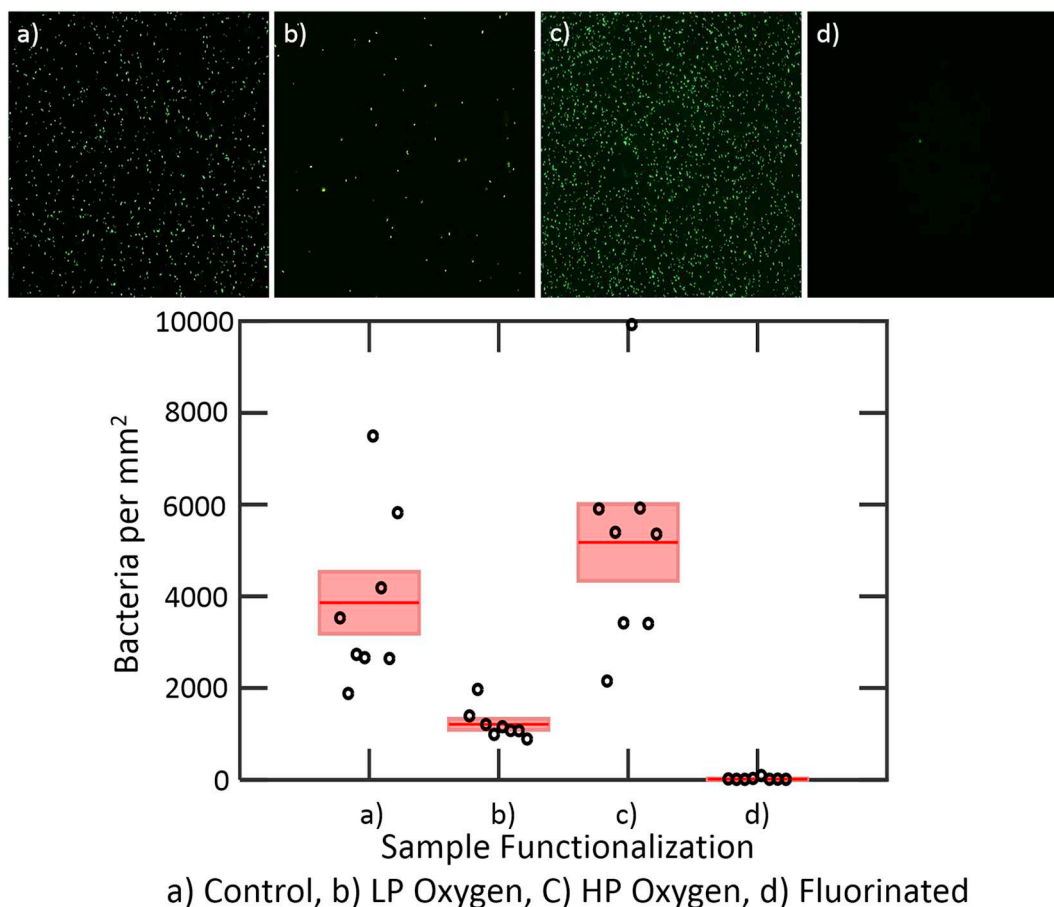**Fig. 5.** Water contact angle of different samples over time.

Fig. 6. Bacterial counts per mm^2 for differently treated samples and fluorescent images of PP samples with adhered bacteria. Error bars indicate standard error (n = 8). a) Control, b) LP oxygen plasma treated, c) HP oxygen plasma treated, d) Fluorinated plasma treated.

samples were also observed to be chemically stable in ambient conditions for over a week. XPS analysis was conducted after one week from the time of sample preparation and showed negligible change in atomic percentage of fluorine, demonstrating that the fluorine ions on the surface are stably bounded from polar covalent carbon-fluorine bonds formed after treatment (Supplement Fig. S5).

3.3. Results of bacterial adhesion tests

Fig. 6 shows the results of the bacterial adhesion experiments and fluorescent representative images of different treated samples with bacteria. Bacterial adhesion was evaluated by fluorescent optical microscopy. Afterwards, ImageJ software was used to count the number of bacteria cells that adhered to the surface. The number of bacteria cells per millimeter squared is plotted for each sample type. Eight coupons were characterized for each RIE treatment. The red solid line represents the mean count, the pink region represents the standard error around the mean, and the black circles represent individual data points. Results show the difference between the LP oxygen treated samples (1209 $\pm$ 120 cells/mm^2) and the HP oxygen treated samples (5176 $\pm$ 835 cells/mm^2).

The LP oxygen treated samples exhibit a decrease in adhered bacteria compared with the control. The decreased bacteria adhesion in these samples is because the hydrophilic surface energetically maintains a liquid barrier between the surface and the bacteria cells, hindering cell-to-surface contact [42,43]. On the other hand, the adhesion of *E. coli* to the HP oxygen treated samples was much more than the control samples. While the surface energies of both types of samples are similar (Table 1), the surfaces of HP oxygen treated samples consist of

dense nanofibrils in contrast to the relatively flat LP oxygen treated samples. The power spectral density of HP oxygen treated samples show a significantly higher frequency of roughness across all roughness wavelengths compared to the relatively flat LP oxygen sample. Bacteria cells adhere more to the HP oxygen samples due to the increased wavelength roughness that is equivalent or larger than *E. coli* cells (rod-shaped about 2 μm long and diameter 0.25 to 1 μm). This roughness increases surface to cell binding sites. Furthermore, the HP oxygen samples contain air pockets that may decrease the effectiveness of the liquid barrier between the bacteria cells and surface. Indeed, these air pockets are why the water contact angle of the HP oxygen surfaces increase over that of LP oxygen surfaces.

The best results were obtained with fluorine plasma treated samples, which are lotus leaf-like. Lotus leaf surfaces are superhydrophobic due to their micron-sized papillae with nanometer-size protrusions and low surface-energy layer of epicuticular wax [44]. These structures are known to resist fouling from soil or dust [45–47]. Likewise, our treatment creates hierarchical microstructure/nanofibrils from a fluorine plasma etch process and the fluorination provides low surface energy. These PP surfaces exhibit lotus-leaf wetting due to a combination of high water static contact angle and low hysteresis. The number of bacteria cells adhered to the fluorinated samples (15 $\pm$ 10 cells/mm^2) was extremely low, 99.6% less than the control samples (3860 $\pm$ 673 cells/mm^2). Under the fluorescent microscope, barely any bacteria cells could be seen on these samples. The nanofibrils are smaller in size than bacteria and together with low surface energy significantly reduce the number of adhesion sites for *E. coli* cells. These fluorinated PP samples emulate the lotus leaf's self-cleaning ability. Statistical analysis was done to evaluate the significance of the anti-

biofouling performance of the various samples. The *p* values were 0.006, 0.242, and 0.001 when the control was compared to the LP oxygen treated samples, HP oxygen treated samples, and the super-hydrophobic, lotus-leaf like fluorine treated samples, respectively.

4. Conclusion

We studied how reactive ion etching modifies the surface of PP samples and affects bacterial adhesion. The effect of different reactive ion etching recipes on morphology, surface energy, and wettability was also investigated. The bacteria adhesion on the LP oxygen treated samples was significantly lower compared to the HP oxygen treated samples. The best anti-biofouling results were obtained from fluorine reactive ion etched samples that created lotus leaf-like hierarchical structures consisting of microstructures and nanofibrils. These PP surfaces exhibit super hydrophobicity, low hysteresis, and 99.6% less adhesion of *E. coli* than control samples. The combination of low surface energy and hierarchical morphology reduces the number of active sites for *E. coli* to adhere to the treated PP, emulating the lotus leaf self-cleaning effect.

Appendix A. Supplementary data

Supplementary data to this article can be found online at https://doi.org/10.1016/j.reactfunctpolym.2018.04.013.

References

[1] G. Akovali, Plastics Rubber and Health, Smithers Rapra Press, 2008.
[2] E.T.J. Rochford, et al., Bacterial adhesion to orthopaedic implant materials and a novel oxygen plasma modified PEEK surface, Colloids Surf. B: Biointerfaces 113 (2014) 213–222.
[3] K. Page, M. Wilson, I.P. Parkin, Antimicrobial surfaces and their potential in reducing the role of the inanimate environment in the incidence of hospital-acquired infections, J. Mater. Chem. 19 (2009) 3819–3831.
[4] A.Y. Peleg, D.C. Hooper, Hospital-acquired infections due to gram-negative Bacteria, N. Engl. J. Med. 362 (2010) 1804–1813.
[5] L.G. Glance, P.W. Stone, D.B. Mukamel, A.W. Dick, Increases in mortality, length of stay, and cost associated with hospital-acquired infections in trauma patients, Arch. Surg. Chic. Ill 1960 (146) (2011) 794–801.
[6] Hospital-Acquired Infections, Practice Essentials, Background, Pathophysiology, (2017).
[7] H.A. Maddah, H.A. Maddah, Polypropylene as a promising plastic: a review, Am. J. Polym. Sci. 6 (2016) 1–11.
[8] Material Science and Engineering: Proceedings of the 3rd Annual 2015 International Conference on Material Science and Engineering (ICMSE2015, Guangzhou, Guangdong, China, 15–17 May 2015), CRC Press, 2016 Available at https://www.crcpress.com/Material-Science-and-Engineering-Proceedings-of-the-3rd-Annual-2015-International/Chen/p/book/9781138029361 , Accessed date: 29 May 2017.
[9] M. Sandholzer, K. Bernreitner, K. Klimke, C.H. Holzer, M. Payer, Polypropylene and polypropylene-elastomer blends for medical packaging, AIP Conf. Proc. 1779 (2016) 110001.
[10] M. Râpă, E. Matei, P.N. Ghioca, C. Cincu, M. Niculescu, Structural changes of modified polypropylene with thermoplastic elastomers for medical devices applications, J. Adhes. Sci. Technol. 30 (2016) 1727–1740.
[11] P.L. Tran, et al., Organoselenium Polymer Inhibits Biofilm Formation in Polypropylene Contact Lens Case Material, Eye Contact Lens 43 (2017) 110.
[12] P.B.J. Vermeltfoort, J.M.M. Hooymans, H.J. Busscher, H.C. Van Der Mei, Bacterial transmission from lens storage cases to contact lenses—effects of lens care solutions and silver impregnation of cases, J. Biomed. Mater. Res. B Appl. Biomater. 87B (2008) 237–243.
[13] Medical Plastics Market Size By Application | Industry Report 2014–2025, Available at http://www.grandviewresearch.com/industry-analysis/medical-plastics-market , Accessed date: 27 September 2017.
[14] A.Q. Le, et al., Preparation of polypropylene/silver nano-zeolite plastics and evaluation of antibacterial and mechanical properties, Int. J. Compos. Mater. 6 (2016) 89–94.
[15] K. Delgado, R. Quijada, R. Palma, H. Palza, Polypropylene with embedded copper metal or copper oxide nanoparticles as a novel plastic antimicrobial agent, Lett. Appl. Microbiol. 53 (2011) 50–54.
[16] H. Palza, et al., Toward tailor-made biocide materials based on poly(propylene)/ copper nanoparticles, Macromol. Rapid Commun. 31 (2010) 563–567.
[17] E. Fages, J. Pascual, O. Fenollar, D. García-Sanoguera, R. Balart, Study of antibacterial properties of polypropylene filled with surfactant-coated silver nanoparticles, Polym. Eng. Sci. 51 (2011) 804–811.
[18] P. Suktha, K. Lekpet, P. Siwayaprahm, M. Sawangphruk, Enhanced mechanical properties and bactericidal activity of polypropylene nanocomposite with dual-function silica–silver core-shell nanoparticles, J. Appl. Polym. Sci. 128 (2013) 4339–4345.
[19] A. Störmer, J. Bott, D. Kemmer, R. Franz, Critical review of the migration potential of nanoparticles in food contact plastics, Trends Food Sci. Technol. 63 (2017) 39–50.
[20] S.A. Ntim, T.A. Thomas, T.H. Begley, G.O. Noonan, Characterisation and potential migration of silver nanoparticles from commercially available polymeric food contact materials, Food Addit. Contam. Part A 32 (2015) 1003–1011.
[21] J. Fabrega, S.N. Luoma, C.R. Tyler, T.S. Galloway, J.R. Lead, Silver nanoparticles: behaviour and effects in the aquatic environment, Environ. Int. 37 (2011) 517–531.
[22] S. Pillai, et al., Linking toxicity and adaptive responses across the transcriptome, proteome, and phenotype of Chlamydomonas reinhardtii exposed to silver, Proc. Natl. Acad. Sci. 111 (2014) 3490–3495.
[23] I. Chopra, The increasing use of silver-based products as antimicrobial agents: a useful development or a cause for concern? J. Antimicrob. Chemother. 59 (2007) 587–590.
[24] Y.-F. Yang, Y. Li, Q.-L. Li, L.-S. Wan, Z.-K. Xu, Surface hydrophilization of microporous polypropylene membrane by grafting zwitterionic polymer for anti-biofouling, J. Membr. Sci. 362 (2010) 255–264.
[25] E. Jafari Nodoushan, N.G. Ebrahimi, M. Ayazi, An anti-bacterial approach to nanoscale roughening of biomimetic rice-like pattern PP by thermal annealing, Appl. Surf. Sci. 423 (2017) 1054–1061.
[26] Standard Classification System and Basis for Specification for Polypropylene Injection and Extrusion Materials, ASTM International, West Conshohocken, PA, 2017, https://doi.org/10.1520/D4101-17 (17).
[27] Standard test method for linear dimensional changes of nonrigid thermoplastic sheeting or film at elevated temperature, ASTM International, West Conshohocken, PA, 2014, https://doi.org/10.1520/D1204 (14).
[28] B.J. Bachmann, Pedigrees of some mutant strains of Escherichia coli K-12, Bacteriol. Rev. 36 (1972) 525–557.
[29] B.P. Cormack, R.H. Valdivia, S. Falkow, FACS-optimized mutants of the green fluorescent protein (GFP), Gene 173 (1996) 33–38.
[30] G. Bertani, Studies on lysogenesis. I. The mode of phage liberation by lysogenic, J. Bacteriol. 62 (1951) 293–300.
[31] R.M.Q. Shanks, J.L. Sargent, R.M. Martinez, M.L. Graber, G.A. O'Toole, Catheter lock solutions influence staphylococcal biofilm formation on abiotic surfaces, Nephrol. Dial. Transplant. 21 (2006) 2247–2255.
[32] D.R. Absolom, et al., Surface thermodynamics of bacterial adhesion, Appl. Environ. Microbiol. 46 (1983) 90–97.
[33] H. Miao, C. Jierong, Inactivation of Escherichia coli and properties of medical poly (vinyl chloride) in remote-oxygen plasma, Appl. Surf. Sci. 255 (2009) 5690–5697.
[34] K. Yamauchi, et al., Antibacterial activity of hydrophobic composite materials containing a visible-light-sensitive photocatalyst, J. Nanotechnol. (2011), https://doi.org/10.1155/2011/380979.
[35] T.D.B. Jacobs, T. Junge, L. Pastewka, Quantitative characterization of surface topography using spectral analysis, Surf. Topogr. Metrol. Prop. 5 (2017) 013001.
[36] M. Flemming, L. Coriand, A. Duparré, Ultra-hydrophobicity through stochastic surface roughness, J. Adhes. Sci. Technol. 23 (2009) 381–400.
[37] B.-S. Kim, N. Bernet, P. Sunderland, J.-A. Manson, Numerical analysis of the dimensional stability of thermoplastic composites using a thermoviscoelastic approach, J. Compos. Mater. 36 (2002) 2389–2403.
[38] Y.F. Huang, C. Huang, Y.L. Zhong, S.P. Yi, Preparing superhydrophobic surfaces with very low contact angle hysteresis, Surf. Eng. 29 (2013) 633–636.
[39] M. Żenkiewicz, Methods for the Calculation of Surface Free Energy of Solids, (2007), p. 24.
[40] F.M. Fowkes, Donor-acceptor interactions at interfaces, J. Adhes. 4 (1972) 155–159.
[41] F.M. Fowkes, Attractive forces at interfaces, Ind. Eng. Chem. 56 (1964) 40–52.
[42] Y. Yuan, P. Hays, M.R. Hardwidge, J. Kim, Surface characteristics influencing bacterial adhesion to polymeric substrates, RSC Adv. 7 (2017) 14254–14261.
[43] S. BinAhmed, A. Hasane, Z. Wang, A. Mansurov, S. Romero-Vargas Castrillón, Bacterial adhesion to ultrafiltration membranes: role of hydrophilicity, natural organic matter, and cell-surface macromolecules, Environ. Sci. Technol. 52 (2018) 162–172.
[44] W. Barthlott, C. Neinhuis, Purity of the sacred lotus, or escape from contamination in biological surfaces, Planta 202 (1997) 1–8.
[45] M. Zhang, S. Feng, L. Wang, Y. Zheng, Lotus effect in wetting and self-cleaning, Biotribology 5 (2016) 31–43.
[46] L. Zhang, Z. Zhou, B. Cheng, J.M. DeSimone, E.T. Samulski, Superhydrophobic behavior of a perfluoropolyether lotus-leaf-like topography, Langmuir 22 (2006) 8576–8580.
[47] Y. Liu, et al., Artificial lotus leaf structures from assembling carbon nanotubes and their applications in hydrophobic textiles, J. Mater. Chem. 17 (2007) 1071–1078.